Effects of Interdiffusion-Induced Strain in $Ga_{0.51}In_{0.49}P$–GaAs Intermixed Quantum Wells

Joseph Micallef, *Member, IEEE*, Andrea Brincat, and Wai-Chee Shiu

Abstract—**The effects of interdiffusion and strain introduced by interdiffusion in lattice-matched GaInP–GaAs single quantum wells are investigated using an error function distribution to model the compositional profile after interdiffusion. Group-III only and dominant group-III interdiffusion produce a large strain build up at the interface, with compressive strain in the well, and tensile strain in the barrier. In the case of group-III only interdiffusion, an abrupt carrier confinement profile is maintained even after significant interdiffusion, with a double- welled bottom, and a potential buildup in the barrier near the interface. Group-V only and group-V dominant interdiffusion again cause a large strain buildup at the interface, with tensile strain in the well and compressive strain in the barrier. Degeneracy of the heavy-hole and light-hole ground states can be achieved, and the electron–light-hole ground state transition energy can also become the effective bandgap energy of the intermixed structure. The model results are consistent with reported experimental results, and show that the effects of the interdiffusion-induced strain on the carrier confinement profiles can be of interest for various quantum-well device applications in this material system, including intersubband infrared photodetectors, polarization-insensitive electroabsorption modulators, and lasers.**

Index Terms—**$Ga_{0.51}In_{0.49}P$–GaAs, quantum-well intermixing, strain.**

I. Introduction

LATTICE MATCHING of $Ga_{0.51}In_{0.49}P$ to GaAs has been investigated for a number of electronic devices, such as high-speed heterojunction bipolar transistors [1], and field-effect transistors [2], as well as photonic applications including light-emitting diodes [3], tandem solar cells [4], visible heterostructure lasers [5], and infrared quantum well (QW) intersubband photodetectors [6]. GaInP lattice-matched to GaAs has received considerable attention also as a potential substitute of AlGaAs layers, in electronic and photonic devices. GaInP is not as readily oxidized as AlGaAs and does not suffer from a high concentration of deep trap centers that result from the presence of oxygen. The GaInP–GaAs interface exhibits very low recombination velocity [7] compared to the AlGaAs–GaAs interface, which should be of advantage in photodetector applications.

Manuscript received February 3, 1998.

J. Micallef and A. Brincat are with the Department of Microelectronics, University of Malta, Msida MSD 06, Malta.

W.-C. Shiu is with the Department of Mathematics, Hong Kong Baptist University, Waterloo Road, Hong Kong.

Publisher Item Identifier S 1077-260X(98)06796-3.

Selective intermixing of QW structures is being actively investigated with two principal objectives: obtaining high-performance device applications and achieving monolithic integration. Interdiffusion of the constituent atoms across the well-barrier interfaces takes place during the intermixing process [8], resulting in modified confinement profiles and subband edge structure. The extent of interdiffusion is a function of the QW intermixing technique parameters, such as the nature and concentration of the impurity species present, and the process temperature and time. QW intermixing has been used to produce lateral photon confinement in lasers and optical waveguides [9], obtain improved performance and wavelength tuning in GaAs-based [10], [11] and InP-based laser structures [12], as well as implement a polarization-insensitive InGaAs–InGaAsP–InP amplifier [13].

Intermixing of lattice-matched GaInP–GaAs QW structures can result in the interdiffusion of both group-III (Ga, In) and group-V (P, As) atoms. Experimental results of thermal interdiffusion of lattice-matched GaInP–GaAs QW's have been interpreted in terms of substantial interdiffusion of the group-III atoms together with minor interdiffusion of group-V atoms [14]. The intermixed structure may or may not be lattice-matched to GaAs; if the rates of interdiffusion on the two sublattices are not comparable, then a strained-layer structure will result, so that strain can be introduced into lattice-matched GaInP–GaAs QW structures by means of postgrowth intermixing. As in the case of the intermixing of lattice-matched InGaAs–InP QW's both compressive and tensile strain can result from the intermixing process.

Strain and interdiffusion both have, independently, important potential applications in several quantum-well (QW) photonic devices, particularly in the case of lasers and amplifiers [15], [16], waveguides [10], modulators [17], and infrared detectors [18], while interdiffusion also facilitates monolithic integration [19]. The possibility of combining the effects of strain and interdiffusion can provide a more powerful tool for the bandgap engineering that is required for device performance optimization and for photonic and optoelectronic integration. In order to optimize the interdiffusion process so as to exploit fully the potential of QW intermixing, detailed modeling of the compositional, strain, and carrier confinement profiles after intermixing is required. In this paper, we first present details of the model used, incorporating strain and its effects, where appropriate, in order to arrive at the carrier confinement profile and sub-

band edge structure of the interdiffused GaInP–GaAs QW. Compositional, strain, and carrier confinement profiles, and the subband edge structure are then presented and discussed for the interdiffusion conditions that can introduce strain, namely, group-III only interdiffusion, dominant group-III interdiffusion, dominant group-V interdiffusion, and group-V only interdiffusion.

II. Computational Details

Consider an undoped GaAs layer lattice-matched to semi-infinite $Ga_{0.51}In_{0.49}P$ barriers. The interdiffusion of Ga and In atoms is characterized by a diffusion length $L_{d(\mathrm{III})}$, which is defined as $L_{d(\mathrm{III})} = (Dt)^{1/2}$, where D is the diffusion coefficient and t is the diffusion time; the interdiffusion of P and As atoms is characterized by a different diffusion length $L_{d(\mathrm{V})}$. When $L_{d(\mathrm{III})} = L_{d(\mathrm{V})}$ the QW structure remains lattice-matched. For group-III only interdiffusion $L_{d(\mathrm{V})} = 0$, for group-V only interdiffusion $L_{d(\mathrm{III})} = 0$, while $L_{d(\mathrm{V})} \neq L_{d(\mathrm{III})}$ represents interdiffusion on the two sublattices but at different interdiffusion rates. In all these cases, strain is introduced into the QW structure and its effects must therefore be modeled in order to arrive at the final carrier confinement profiles.

The band structure of bulk III–V compound semiconductors is characterized by a conduction band with light effective mass, a valence band that is doubly degenerate at the Brillouin zone center Γ, and a spin–orbit splitoff valence band. The doubly degenerate bands are identified as the heavy-hole (HH) and light-hole (LH) bands due to their different effective masses.

If the QW layer thickness is within the critical thickness regime, the QW structure will be coherently strained after interdiffusion, with a biaxial hydrostatic strain parallel to the well-barrier interface and a uniaxial shear strain perpendicular to the interface. The band structure is modified by the presence of strain. The biaxial component of strain alters the bulk bandgap between the conduction band and both the degenerate valence bands and the spin–orbit splitoff valence band. The uniaxial component of the strain lifts the degeneracy of the HH and LH bands at Γ. In the case of compressive strain the biaxial component causes an increase in the bulk bandgap energy, while the uniaxial component shifts the HH band toward the conduction band and the LH band away from the conduction band [20]. This valence band splitting is increased by the quantum-size effects in the case of compressive strain. In the case of tensile strain, the biaxial component decreases the bulk band gap energy while the uniaxial component causes the HH band to shift away from the conduction band and the LH band to move toward the conduction band. The quantum size effects now reduce the valence band splitting. The uniaxial component also causes the LH band to couple with the spin–orbit splitoff band [21].

The constituent atoms compositional profile after the intermixing process is modeled using an error function distribution [22]. The compositional profiles after interdiffusion can thus be represented as follows.

1) In the group-III sublattice, the In concentration after interdiffusion, $\tilde{x}(z)$, is described by

$$\tilde{x}(z) = x\left(1 - \frac{1}{2}\left[\mathrm{erf}\left(\frac{L_z + 2z}{4L_{d(\mathrm{III})}}\right) + \mathrm{erf}\left(\frac{L_z - 2z}{4L_{d(\mathrm{III})}}\right)\right]\right) \tag{1}$$

where x is the In concentration of the as-grown structure, L_z is the as-grown well width, z is the growth direction, and the QW is centered at $z = 0$.

2) in the group-V sublattice, the As compositional profile after interdiffusion $\tilde{y}(z)$ is described by

$$\tilde{y}(z) = \frac{y}{2}\left[\mathrm{erf}\left(\frac{L_z + 2z}{4L_{d(\mathrm{V})}}\right) + \mathrm{erf}\left(\frac{L_z - 2z}{4L_{d(\mathrm{V})}}\right)\right] \tag{2}$$

where $y = 1$ is the As concentration of the as-grown well.

The compositional profile in the QW structure after interdiffusion implies that the carrier effective mass, the bulk (unstrained) bandgap, and the biaxial and uniaxial components of strain vary continuously across the QW. Consequently, the carrier effective mass, $m_r^*(z)$, is now z-dependent and is obtained from $m_r^*(z) = m_r^*(\tilde{x}, \tilde{y})$, where $m_r^*(x, y)$ is the respective carrier bulk effective mass, and r denotes either the electron (C), HH (V = HH), or LH (V = LH). The unstrained (bulk) bandgap in the well, $E_g(\tilde{x}, \tilde{y})$, is also a function of the compositional profile, so that the unstrained potential profile after interdiffusion $\Delta E_r(\tilde{x}, \tilde{y})$ varies across the well and is given by

$$\Delta E_r(\tilde{x}, \tilde{y}) = Q_r \Delta E_g(\tilde{x}, \tilde{y}) \tag{3}$$

where Q_r is the band offset and ΔE_g is the unstrained bandgap offset.

The in-plane strain across the well will also vary so that the strain effects are also z-dependent. The QW confinement potential after the intermixing process, obtained by modifying the bulk postprocessing potential profile with the variable strain effects, is therefore given by

$$U_r(z) = Q_r[\Delta E_g(\tilde{x}, \tilde{y}) - S_\perp(\tilde{x}, \tilde{y})] \pm S_{\|r}(\tilde{x}, \tilde{y}) \tag{4}$$

where $S_\perp(\tilde{x}, \tilde{y})$ represents the change in the bulk bandgap due to the biaxial component of strain, $S_{\|r}(\tilde{x}, \tilde{y})$ represents the splitting energy between the HH and LH band edges induced by the uniaxial component of strain, with the +ve sign representing the confined HH profile and the −ve sign representing the confined LH profile, $S_{\|lh}(\tilde{x}, \tilde{y})$ includes the effect of the LH band coupling with the splitoff band, and $S_{\|c}(\tilde{x}, \tilde{y}) = 0$.

Equation (4) represents the carrier confinement profiles for the general case of an intermixed GaInP–GaAs QW structure, where interdiffusion on both sublattices takes place, but at different rates. In the case of comparable interdiffusion on the two sublattices (4) reduces to

$$U_r(z) = \Delta E_r(\tilde{x}, \tilde{y}). \tag{5}$$

In the case of interdiffusion taking place only on the group-III sublattice (4) becomes

$$U_r(z) = \Delta E_r(\tilde{x}, 1) - S_{\perp r}(\tilde{x}, 1) \pm S_{\|r}(\tilde{x}, 1) \tag{6}$$

while for interdiffusion on group-V sublattice only the carrier confinement profiles are given by

$$U_r(z) = \Delta E_r(0,\tilde{y}) - S_{\perp r}(0,\tilde{y}) \pm S_{\parallel r}(0,\tilde{y}). \quad (7)$$

The electron and hole subband structure at Γ can be determined by considering the appropriate Schrödinger equation from the BenDaniel–Duke model [23], using the envelope function scheme [24] with an effective mass approximation. The one-electron Schrödinger equation for the disordered QW can be expressed as

$$\frac{-\hbar^2}{2}\frac{d}{dz}\left(\frac{1}{m_r^*(z)}\frac{d\chi_{r\ell}(z)}{dz}\right) + U_r(z)\chi_{r\ell}(z) = E_{r\ell}\chi_{r\ell}(z) \quad (8)$$

where the growth direction z is the confinement axis, $\chi_{r\ell}(z)$ is the envelope wavefunction, $E_{r\ell}$ is the quantized energy level with the subband energy zero at the bottom of the QW, and $\ell = p$ or q refers to the quantized subband energy levels for the electron and holes, respectively. This equation is solved numerically to obtain the quantized energy levels (E_{Cp}, E_{Vq}), and the envelope wavefunctions (χ_{Cp}, χ_{Vq}). Hence the interband transitions energy can be determined, as well as the overlap integral $\langle \chi_{Vq} \mid \chi_{Cp} \rangle$ between the pth conduction subband and the qth valence subband envelope functions, where

$$\langle \chi_{Vq} \mid \chi_{Cp} \rangle = \int_{-z_b}^{z_b} \chi_{Vq}^*(z)\chi_{Cp}(z)\,dz \quad (9)$$

z_b is taken as the boundary where $\chi_{r\ell}(z_b) \to 0$.

The electron–HH transition energy $E_{\mathrm{chh}pq}$ and the electron-LH transition energy $E_{\mathrm{clh}pq}$ can then be obtained from

$$\begin{aligned} E_{cp\mathrm{hh}q} &= E_{g\mathrm{hh}}[\tilde{x}(0),\tilde{y}(0)] + E_{cp} + E_{\mathrm{hh}q} \\ E_{cp\mathrm{lh}q} &= E_{g\mathrm{lh}}[\tilde{x}(0),\tilde{y}(0)] + E_{cp} + E_{\mathrm{lh}q} \end{aligned} \quad (10)$$

respectively, where $E_{g\mathrm{hh}}(\tilde{x}(0),\tilde{y}(0))$ and $E_{g\mathrm{lh}}(\tilde{x}(0),\tilde{y}(0))$ are the electron–HH and electron–LH lowest direct bandgap at Γ after disordering, respectively.

III. Results and Discussion

The structure considered here is an undoped 6-nm-thick GaAs layer sandwiched between semiinfinite $Ga_{0.51}In_{0.49}P$ barriers. Parameter k is defined as $k = L_{d(\mathrm{V})}/L_{d(\mathrm{III})}$, so that when $k < 1$ the interdiffusion rate on the group-V sublattice is less than the interdiffusion rate on the group-III sublattice, while for $k > 1$ the group-V sublattice interdiffusion rate is greater than the group-III sublattice rate. The material parameters for the disordered structure are determined by interpolating between the binary parameters. Details of these parameters, and the bulk bandgap and the spin–orbit splitting compositional dependences, are given in [25]. Different experimental techniques have resulted in various values for the conduction band offset Q_c of lattice-matched GaInP–GaAs heterostructures [26]–[28]. A conduction band offset $Q_c = 45\%$ [28] has been used in the calculations.

A. Group-III Only Interdiffusion

For $k = 0$ interdiffusion takes place on the group-III sublattice only. In this case a graded compositional profile results for the Ga and In atoms, while the P and As atoms compositional profile remains abrupt, as shown in Fig. 1(a) for $L_{d(\mathrm{III})} = 0.5$ nm. Ga diffuses into the barrier while In diffuses into the well forming an InGaAs–GaInP interface. Since the InGaAs lattice constant is always less than GaAs, the QW is under compressive strain, while a tensile strain arises in the barrier near the interface since the Ga concentration here is less than the lattice-matching composition of 0.51. The strain profile that is induced by the intermixing process is shown in Fig. 1(b). For $L_z = 6$ nm and $L_{d(\mathrm{III})} = 0.5$ nm a 1.7% compressive strain in the well close to the interface, and a 1.8% tensile strain in the barrier close to the interface result, while the well center is still unstrained since no compositional intermixing has as yet occurred at the center.

The abrupt change in the group-V atoms compositional profiles produces an abrupt bandgap change at the interface from the InGaAs well to the GaInP barrier so that the carrier confinement profiles remain abrupt after interdiffusion, with a well width equal to that of the as-grown QW. The group-III atoms graded compositional profile across the QW structure modifies the shape of the confinement profiles, while the effects of the strain distribution on this bandgap affects both the shape and separation of the conduction and valence bands, and the HH and LH potential wells no longer coincide, Fig. 1(c). In the well, the HH potential profile is shifted toward the electron (C) potential profile, while the LH potential profile is shifted away from the electron potential profile. In the barrier, near the interface, the tensile strain again separates the HH and LH potential profiles, with the HH potential profile shifted away from, and the LH potential profile shifted toward, the electron potential profile. As a result of these strain effects, the C and HH confinement profiles exhibit a double well profile at the bottom of the well, and a double barrier structure similar to a resonant tunnelling structure. In the case of the LH confinement profile, the compositional and strain separation effects tend to balance each other so that the potential buildup at the top of the well is much less pronounced. The central regions at the bottom of the HH and LH wells still coincide since the region is still unstrained for $L_{d(\mathrm{III})} = 0.5$ nm. Numerical results show that eigen states can be supported in the HH double-welled bottom potential, while tunnelling enhancement is possible for the topmost states in both the C and HH wells.

The variation of strain inside the well with interdiffusion is shown in Fig. 2(a). In the initial stages of interdiffusion ($L_{d(\mathrm{III})} \leq 0.5$ nm for the QW under consideration) a large compressive strain builds up in the well near the interface, while the center of the well is still practically unstrained since the compositional change at the center is still minimal. As interdiffusion proceeds In atoms diffuse to the center of the well so that the group-III atoms composition in the center of the well starts to change and the well center becomes compressively strained. For longer interdiffusion, $L_{d(\mathrm{III})} = 4$

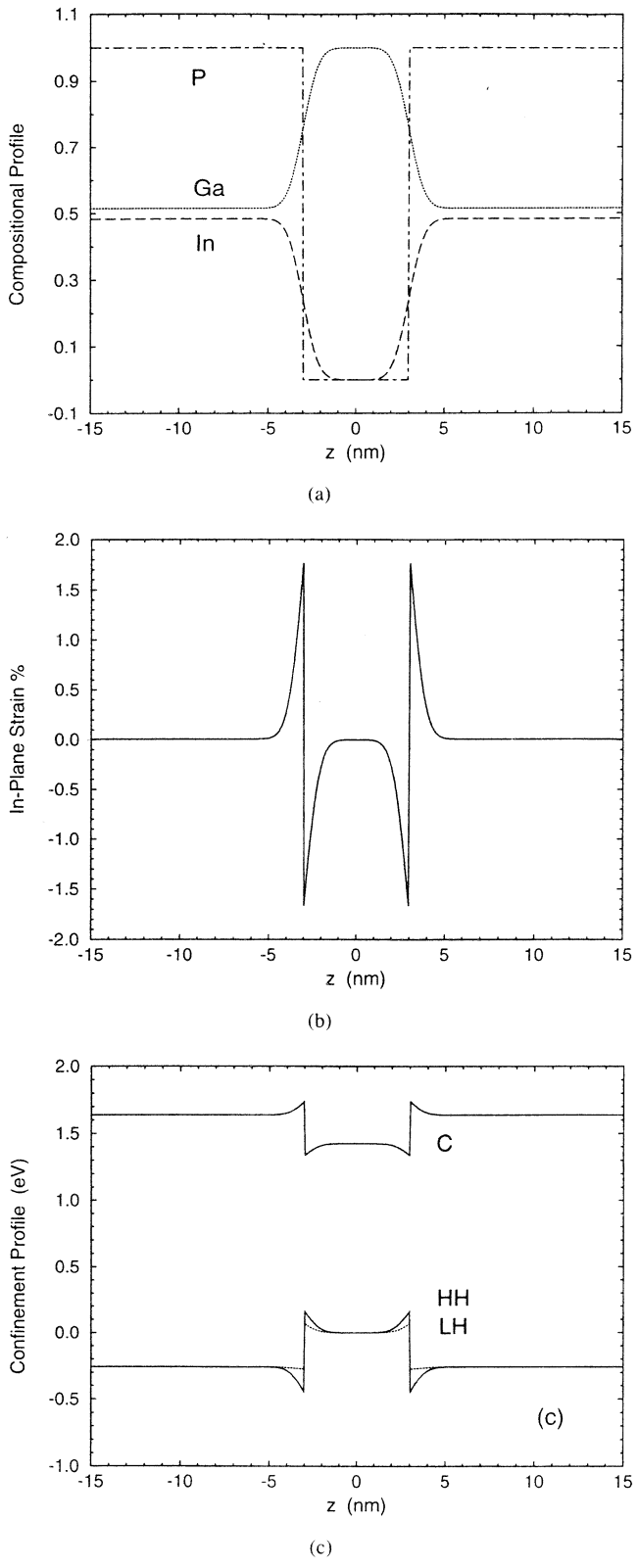

Fig. 1. Profiles of (a) constituent atoms composition, (b) in-plane strain, and (c) carrier confinement potentials for electron (C), HH, and LH, for $L_z = 6$ nm, $L_{d(\mathrm{III})} = 0.5$ nm, $L_{d(\mathrm{V})} = 0$ nm, with well center at $z = 0$.

nm, the strain profile across the QW becomes fairly uniform, mirroring the compositional distribution. The tensile strain in the barrier near the interface remains practically the same as interdiffusion proceeds, Fig. 2(b). In the case of the HH confinement profile, this tensile strain enhances the potential buildup at the top of the well, while in the case of the LH confinement profile the tensile strain effects balance out the potential buildup.

The electron (C) and HH subband-edge structures for $L_{d(\mathrm{III})} = 0.5$ nm are shown in Fig. 3. For the structure considered here, four subband states result in the HH well with the HH ground state lying near the top of the well bottom miniwells. The conduction well, on the other hand, supports two confined subbands. By careful optimization of the intermixing process a first excited state at an energy level close to the continuum can be obtained in the conduction well. Because of the presence of the potential buildup caused by the tensile strain in the barrier close to the interface, the envelope wavefunction of the first excited state would still be fairly well confined, as shown in Fig. 4. With the application of an external electric field, the electron in this first excited state is expected to tunnel out of the conduction well, since the thickness of the potential build up is only about 1 nm. This result could be of interest for intersubband photodetector applications, since GaInP–GaAs QW infrared photodetectors are being actively investigated for long wavelength detection [28], [29].

The ground state electron-HH (C1-HH1) and electron-LH (C1-LH1) transition energy variations with $L_{d(\mathrm{III})}$ are shown in Fig. 5. The effective QW bandgap energy of the intermixed structure is the C1-HH1 transition. As the interdiffusion proceeds the bandgap energy decreases, corresponding to a shift to longer wavelengths, as evidenced in experimental results for thermal intermixing of GaInP–GaAs QW's [14]. The shift to longer wavelengths with interdiffusion is similar to experimental results for Zn-diffusion induced intermixing of $In_{0.53}Ga_{0.47}As$–InP QW's. In contrast, intermixing in AlGaAs–GaAs [22] and InGaAs–GaAs [30] QW structures, where interdiffusion also takes place on the group-III sublattice only, results in bandedge shifts to shorter wavelengths.

B. Interdiffusion on Both Sublattices

For $0 < k < 1$, interdiffusion takes place predominantly on the group-III sublattice, along with minor interdiffusion on the group-V sublattice. Strain is again induced in the intermixed QW structure since $L_{d(\mathrm{V})} \neq L_{d(\mathrm{III})}$, having a similar profile as for $k = 0$, with compressive strain in the well and tensile strain in the barrier close to the interface. For the case $k = 0.25$, $L_{d(\mathrm{III})} = 0.5$ nm, and $L_z = 6$ nm, the strain in the well close to the interface, and in the barrier close to the interface, shows a decrease of about 40% compared to $k = 0$. Since interdiffusion now takes place on the two sublattices the carrier confinement profiles are no longer abrupt, while the double-well potential at the well bottom and the potential build up at the top of the well are much less pronounced.

The variation of the ground state transition energy with interdiffusion, for different values of k, is shown in Fig. 6. The QW bandgap energy is the C1-HH1 transition, reflecting the compressive nature of the strain induced in the QW by the intermixing process. As already noted the bandgap energy decreases for $k = 0$ as the interdiffusion proceeds, corre-

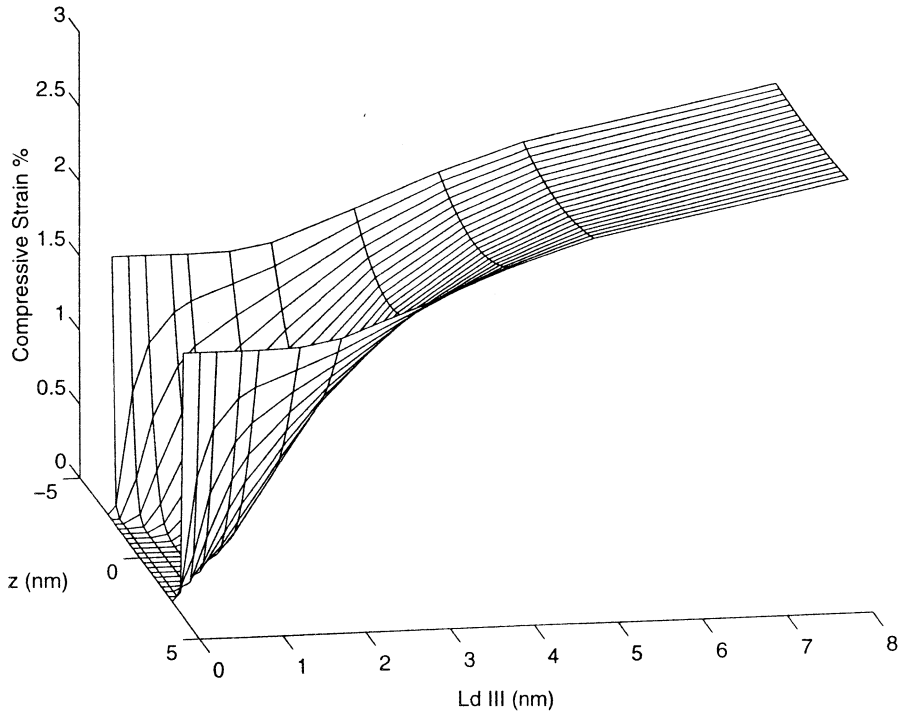

(a)

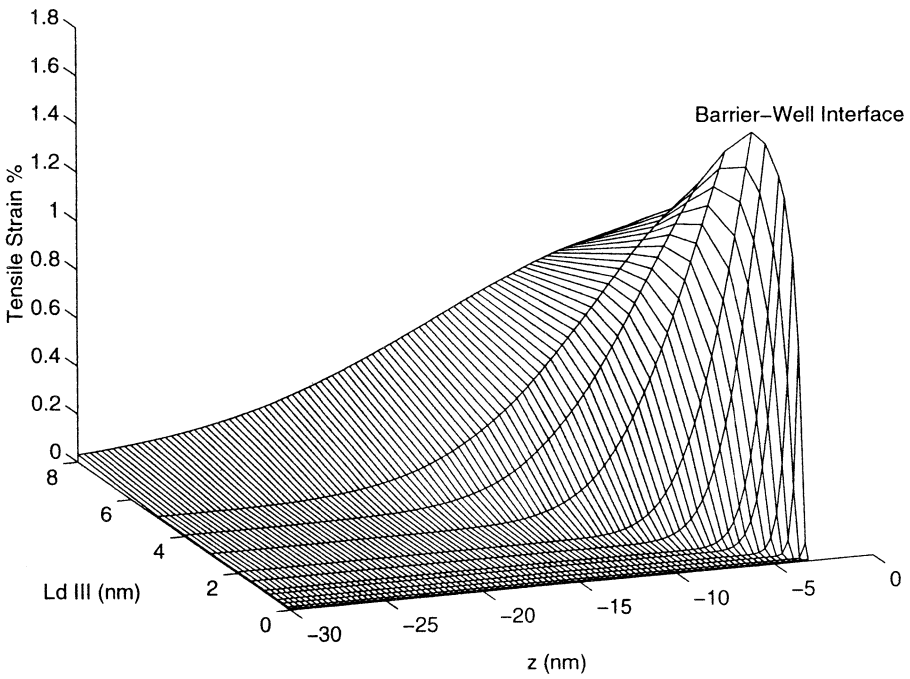

(b)

Fig. 2. Interdiffusion-induced strain in the intermixed GaInP–GaAs structure for group-III sublattice only interdiffusion. (a) Compressive strain distribution in the well. (b) Tensile strain distribution in the barrier close to the interface.

sponding to a large red shift of the effective bandgap of the interdiffused QW. When $k = 0.25$, a red shift in the effective bandgap again results. However, for long enough interdiffusion duration, the red shift saturates and even decreases. The results obtained from our model correspond to experimental results reported for disordering of $Ga_{0.51}In_{0.49}P$–GaAs QW's by thermal annealing [14], showing the red shift saturating and decreasing with increasing duration of the QW disordering process. For $k = 0.5$, the red shift again saturates and then decreases, but at an earlier stage of the interdiffusion process, since the competing group-V sublattice interdiffusion is now more pronounced. Thus for $k < 1$, the ground state transition energy variation (saturation and subsequent decrease of the red shift) provides an indication of how dominant the group-III atoms interdiffusion is with respect to the group-V interdiffusion.

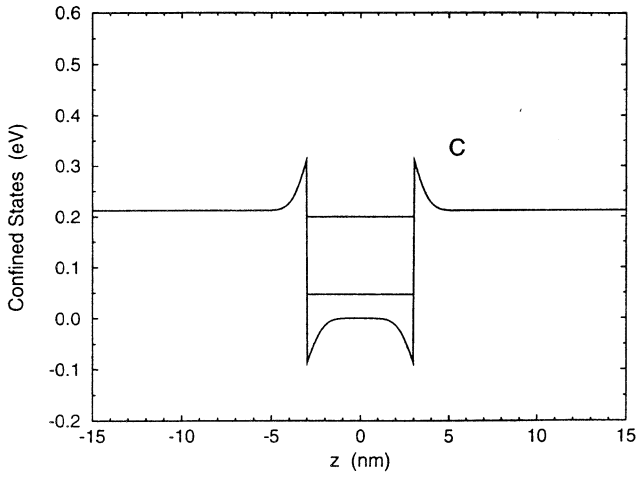

(a)

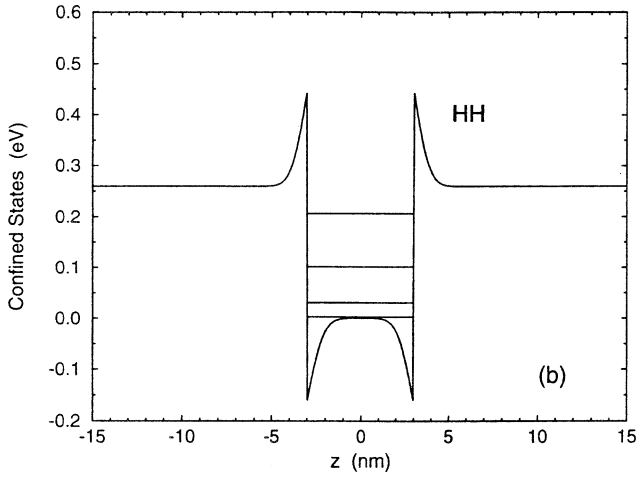

(b)

Fig. 3. (a) Electron and (b) HH bound states for group-III sublattice only interdiffusion with $L_{d(\mathrm{III})} = 0.5$ nm, $L_z = 6$ nm.

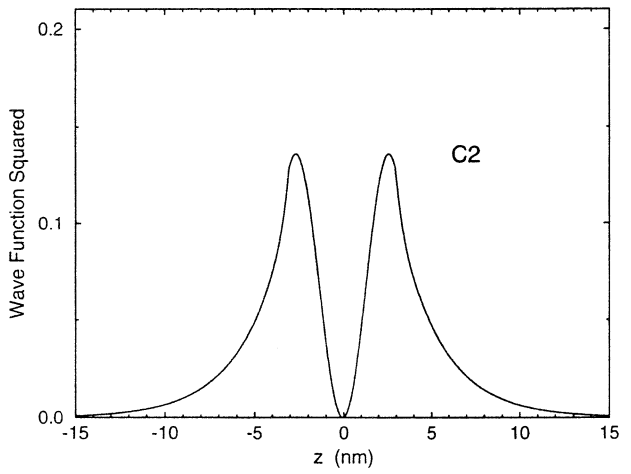

Fig. 4. Envelope wavefunction squared for electron first excited state, considering only group-III sublattice interdiffusion, with $L_{d(\mathrm{III})} = 0.5$ nm.

For $k > 1$ the group-V interdiffusion rate is greater than the group-III interdiffusion rate. The in-plane strain and carrier confinement profiles for the case $L_{d(\mathrm{III})} = 0.5$ nm, $L_{d(\mathrm{V})} =$ 1 nm, are shown in Fig. 7. The compositional profile causes a tensile strain to be set up in the interdiffused well and a compressive strain in the barrier close to the interface, as shown in Fig. 7(a). The combination of the unstrained bandgap and the effects of the strain profile on this bandgap gives rise to the confinement potentials shown in Fig. 7(b). The effects of the tensile strain are also clearly evident in the confinement potential. The tensile strain causes the LH potential profile to shift toward the electron (C) potential profile, while the HH potential profile is now shifted away from the C profile. Fig. 8 shows that the wavefunctions of the electron ground state and first excited state are still fairly well confined.

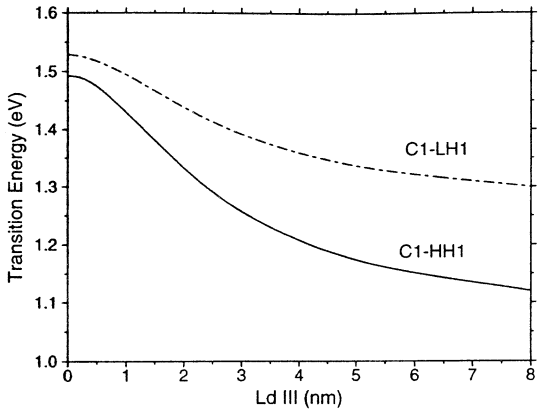

Fig. 5. Variation of ground state transition energy with interdiffusion on the group-III sublattice.

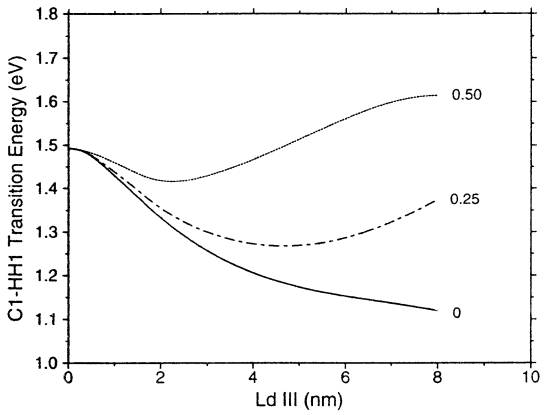

Fig. 6. Electron–HH ground state transition energy with interdiffusion for various values of $k < 1$, where $k = L_{d(\mathrm{V})}/L_{d(\mathrm{III})}$.

The ground state electron-HH (C1-HH1) transition energy variation with $L_{d(\mathrm{III})}$ for different values of $k \geq 1$ are shown in Fig. 9. For interdiffusion length $L_{d(\mathrm{V})} > 2$ nm the material compositional profile inside the well results in carrier confinement profiles that exhibit full double well characteristics, and the effects of prolonged interdiffusion are not considered here in this case. For $0 < L_{d(\mathrm{V})} < 2$ nm the bandgap energy increases, corresponding to a shift to shorter wavelengths. The shift to shorter wavelengths with interdiffusion is similar to experimental results reported for intermixing of $In_{0.53}Ga_{0.47}As$–InP single and multiple QW's induced by thermal annealing at temperatures in the 600 °C to 850 °C range [31].

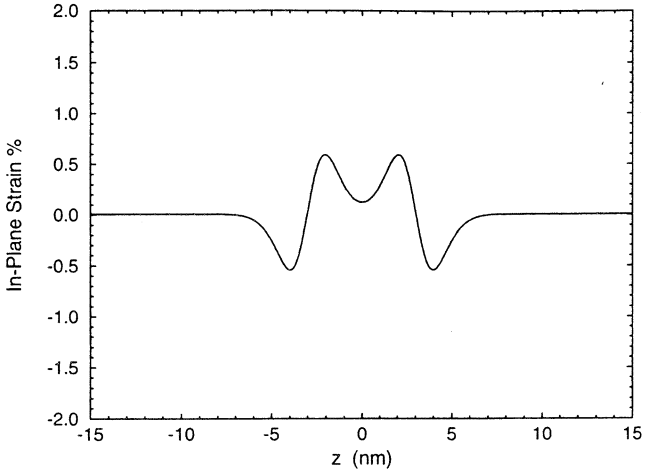

(a)

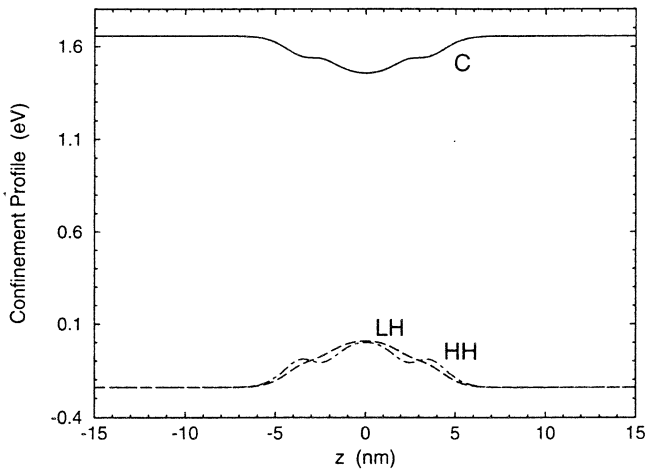

(b)

Fig. 7. Distribution of (a) in-plane strain, and (b) carrier confinement profiles for $L_{d(\mathrm{III})} = 0.5$ nm, $L_{d(\mathrm{V})} = 1$ nm.

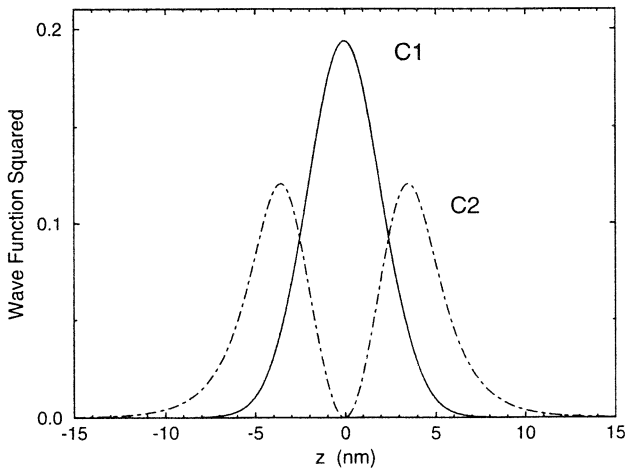

Fig. 8. Envelope wavefunction squared for bound electron states C1 and C2 for intermixed GaInP–GaAs QW with $L_{d(\mathrm{III})} = 0.5$ nm, $L_{d(\mathrm{V})} = 1$ nm.

C. Group-V Only Interdiffusion

Fig. 10 shows the in-plane strain and confinement profiles for the case $L_{d(\mathrm{V})} = 0.5$ nm, $L_{d(\mathrm{III})} = 0$. Since $k > 1$, the strain in the well is tensile, while compressive strain builds up

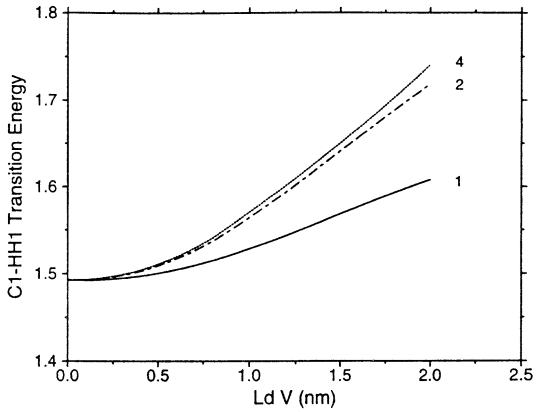

Fig. 9. Electron–HH ground state transition energy variation with interdiffusion for various values of $k > 1$, where $k = L_{d(\mathrm{V})}/L_{d(\mathrm{III})}$.

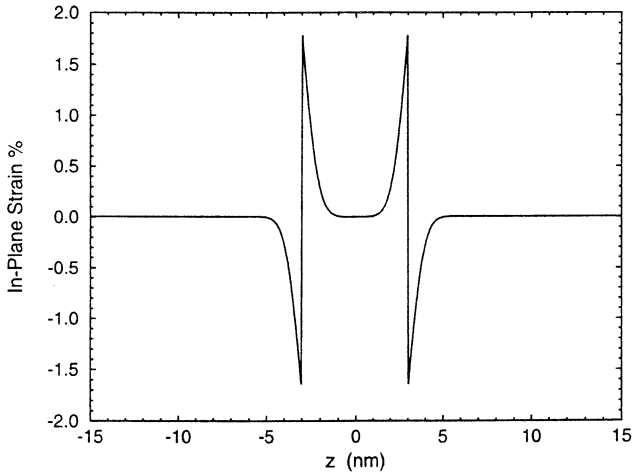

(a)

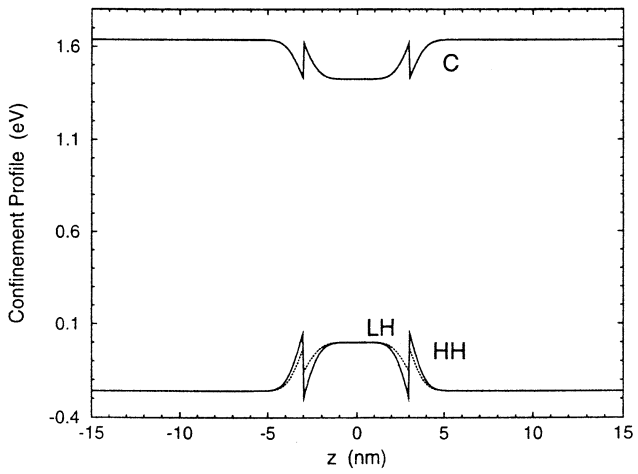

(b)

Fig. 10. Profiles of (a) in-plane strain, and (b) carrier confinement potentials for group-V atoms only interdiffusion, with $L_z = 6$ nm, $L_{d(\mathrm{V})} = 0.5$ nm.

in the barrier near the interface. For this interdiffusion length the well center is still GaAs and there is thus no strain in this region. The effects of this strain profile together with the bandgap profile due to the material composition give rise to the confinement profiles shown. In contrast to the potential buildup in the barrier close to the interface that resulted in

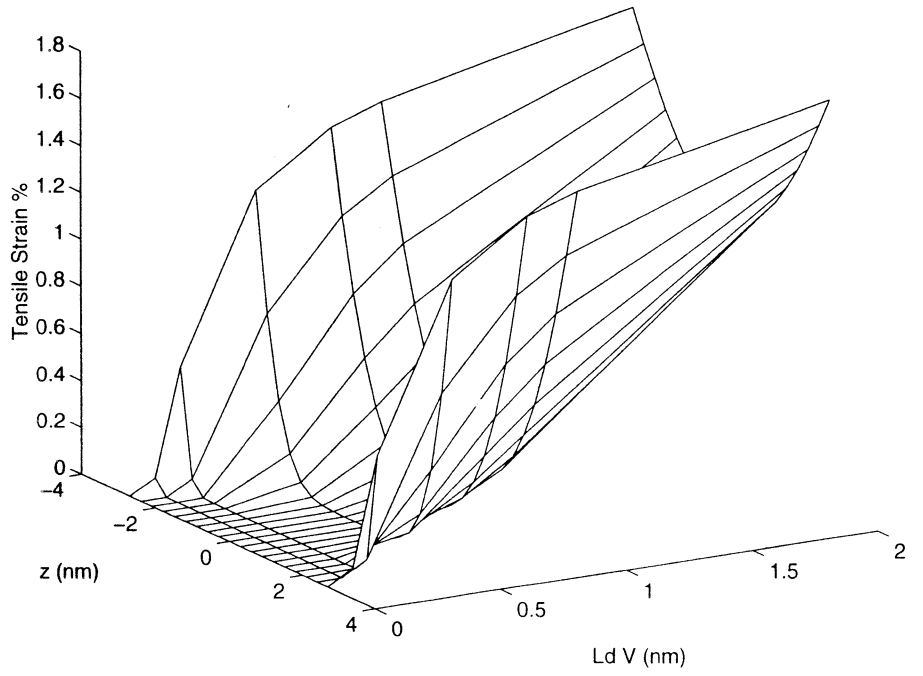

(a)

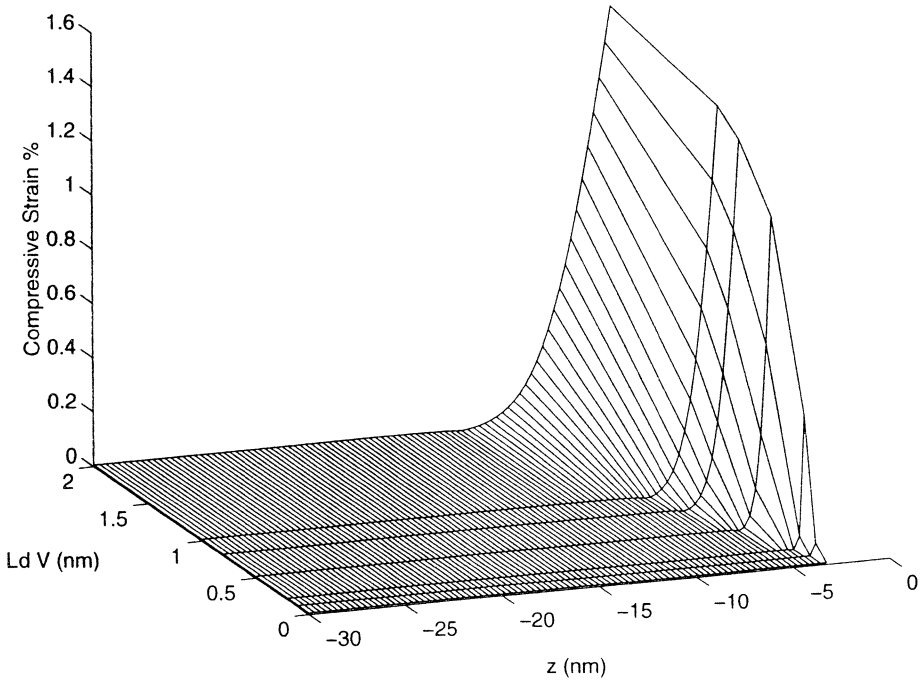

(b)

Fig. 11. Interdiffusion-induced strain in the intermixed GaInP–GaAs structure with interdiffusion on group-V sublattice only. (a) Tensile strain in the well. (b) Compressive strain in the barrier close to the interface.

the case of group-III only interdiffusion, the composition and compressive strain in the barrier close to the interface now give rise to two narrow side wells.

The strain induced in the QW structure by the intermixing process for various values of $L_{d(\mathrm{V})}$ is shown in Fig. 11. In the very early stages of interdiffusion, a large tensile strain results in the well close to the interface, with no strain at the well center, Fig. 11(a). As $L_{d(\mathrm{V})}$ increases, the constituent atoms composition at the center of the well changes so that tensile strain is induced also in the central well region. The barrier close to the interface becomes compressively strained and this strain increases with interdiffusion, Fig. 11(b).

The change in the HH and LH ground state transition energy with interdiffusion length $L_{d(\mathrm{V})}$ is shown in Fig. 12. As interdiffusion proceeds the LH transition energy approaches the HH transition energy and the two converge at $L_{d(\mathrm{V})} = 1.2$ nm. The energy level splitting of the HH and LH ground states due to the different masses is compensated by the effects of the

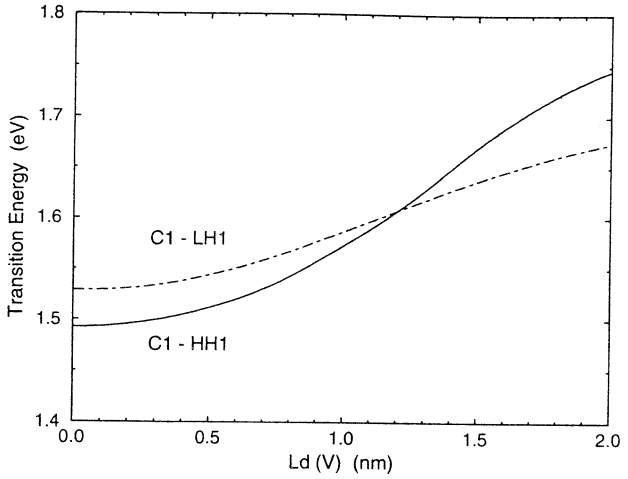

Fig. 12. Ground state transition energy variation with interdiffusion on the group-V sublattice only: electron–HH (solid line), and electron–LH (dotted-dashed line), showing degeneracy of the HH and LH ground states at $L_{d(V)} = 1.2$ nm.

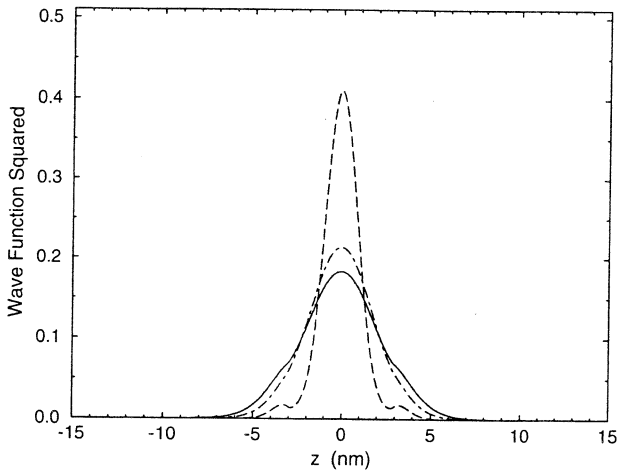

Fig. 13. Envelope wavefunctions squared for C1 (solid line), HH1 (dashed line), and LH1 (dot-dashed line) for group-V sublattice only interdiffusion with $L_{d(V)} = 1.2$ nm.

tensile strain induced in the interdiffused well. For the structure and interdiffusion conditions considered here a 0.25% tensile strain is induced in the center of the well after interdiffusion. The effective bandgap is at the same time increasing with interdiffusion indicating a shift to shorter wavelengths of the absorption edge. This is a result of the changing bandgap between the conduction and hole confinement profiles as modified by the compositional disordering and the induced tensile strain. At $L_{d(V)} = 1.2$ nm the wavefunctions of the ground state electron, HH and LH are still quite well confined, as shown in Fig. 13. Thus, the convergence of the HH and LH ground state transition energies can be exploited to design photonic devices that could exhibit polarization independent properties. A polarization insensitive InGaAs–InGaAsP–InP amplifier has recently been demonstrated [13].

Above $L_{d(V)} = 1.2$ nm the shift to shorter wavelengths continues and the LH ground state transition energy now determines the effective bandgap of the interdiffused structure. This is of interest for laser applications, since a much better performance, than predicted by theory, for lasing from the electron–LH transition in a tensile-strained InGaAs–InP MQW structure has been reported [32].

Our results also show that, depending on the width of the as-grown QW and on the intermixing process conditions, the two above effects can be achieved as long as group-V interdiffusion dominates.

IV. Conclusion

The effects of interdiffusion, and the interdiffusion-induced strain, of lattice-matched $Ga_{0.51}In_{0.49}P$–GaAs QW's have been investigated. Whenever the interdiffusion rates on the group-III and group-V sublattices differ, strain is introduced into the QW structure. The sign of this strain depends on which interdiffusion rate predominates. When interdiffusion takes place on the group-III sublattice only, an abrupt confinement profile is maintained with a well width equal to that of the as-grown quantum well. The compositional intermixing and the effects of the compressive strain inside the well and the tensile strain in the barrier close to the interface give rise to a confinement profile with a double-welled bottom and a potential buildup at the top of the well. This confinement profile is of potential interest in QW intersubband infrared photodetector applications. In the case of group-V only, or group-V dominant, interdiffusion, tensile strain is introduced in the well, with compressive strain in the barrier close to the interface. As a result of the tensile strain in the well, the electron–LH ground state transition energy can be made to coincide with the electron–HH ground state transition energy. This condition opens up the possibility for polarization-insensitive response in QW photonic device applications. Further interdiffusion on the group-V sublattice will result in the electron-LH transition energy becoming the effective bandgap energy, and this result is of importance in lasing applications. The confinement profiles in the case of group-V only interdiffusion are abrupt, but different from those obtained in the case of group-III only interdiffusion. When interdiffusion takes place on both sublattices at a different rate, the confinement profiles are no longer abrupt and the direction of shift of the fundamental absorption edge depends on which sublattice interdiffusion dominates. The introduction of strain by interdiffusion can be exploited in various quantum well photonic applications.

References

[1] J.-I. Song, C. Caneau, K.-B. Chough, and W.-P. Hong, "GaInP/GaAs double heterojunction bipolar transistor with high f_T, f_{max}, and breakdown voltage," *IEEE Electron Device Lett.*, vol. 15, pp. 10–12, 1994.

[2] M. Razeghi, F. Omnes, M. Defour, P. Maurel, P. Bove, Y. J. Chan, and D. Pavlidis, "The first fabrication of n- and p-type $Ga_{0.48}In_{0.52}P$/Ga(In)As lattice-matched and strained HIGFET structures grown by MOCVD," *Semiconduct. Sci. Technol.*, vol. 5, pp. 274–277, 1990.

[3] M. K. Lee, R. H. Horng, and L. C. Haung, "Disorder order-disorder $Ga_{0.5}In_{0.5}P$ visible light-emittimg-diodes," *J. Appl. Phys.*, vol. 72, pp. 5420–5422, 1992.

[4] T. Takamoto, E. Ikeda, H. Kurita, and M. Ohmori, "Over 30% efficient InGaP/GaAs tandem solar cells," *Appl. Phys. Lett.*, vol. 70, pp. 381–383, 1997.

[5] K. Koyabashi, S. Kawata, A. Gomyo, I. Hino, and T. Suzuki, "Room-temperature CW operation of AlGaInP double-heterostructure visible lasers," *Electron. Lett.*, vol. 21, pp. 931–932, 1985.
[6] C. Jelen, S. Slivken, J. Hoff, M. Razeghi, and G. J. Brown, "Aluminum free GaInP/GaAs quantum well infrared photodetectors for long wavelength detection," *Appl. Phys. Lett.*, vol. 70, pp. 360–362, 1997.
[7] J. M. Olsen, R. K. Ahrankiel, D. L. Dunlavy, B. Keys, and A. E. Kibbler, "Ultralow recombination velocity at $Ga_{0.5}In_{0.5}P$/GaAs heterointerfaces," *Appl. Phys. Lett.*, vol. 55, pp. 1208–1210, 1989.
[8] M. D. Camras, N. Holonyak Jr., R. D. Burnham, W. Streifer, D. R. Scifres, T. L. Paoli, and C. Lindström, "Wavelength modification of $Al_xGa_{1-x}As$ quantum well heterostructure lasers by layer interdiffusion," *J. Appl. Phys.*, vol. 54, pp. 5637–5641, 1983.
[9] W. Xia, S. C. Lin, S. A. Pappert, C. A. Hewett, M. Fernandes, T. T. Vu, P. K. L. Yu, and S. S. Lau, "InGaAs/InP superlattice waveguides by elevated temperature argon ion mixing," *Appl. Phys. Lett.*, vol. 55, pp. 2020–2022, 1989.
[10] S. Y. Hu, M. G. Peters, D. B. Young, A. C. Gossard, and L. A. Coldren, "Submilliampere-threshold InGaAs–GaAs quantum-well ridge-waveguide lasers with lateral confinement provided by impurity-induced disordering," *IEEE Photon. Technol. Lett.*, vol. 7, pp. 712–714, 1995.
[11] S. Bürkner, J. D. Ralston, S. Weisser, J. Rosenzweig, E. C. Larkins, R. E. Sah, and J. Fleissner, "Wavelength tuning of high-speed InGaAs-GaAs-AlGaAs pseudomorphic MQW lasers via impurity-free interdiffusion," *IEEE Photon. Technol. Lett.*, vol. 7, pp. 941–943, 1995.
[12] P. J. Poole, S. Charbonneau, M. Dion, G. C. Aers, M. Buchanan, R. D. Goldberg, and I. V. Mitchell, "Demonstration of an ion-implanted wavelength-shifted quantum-well laser," *IEEE Photon. Technol. Lett.*, vol. 8, pp. 16–18, 1996.
[13] J.-J. He, S. Charbonneau, P. J. Poole, G. C. Aers, Y. Feng, E. S. Koteles, R. D. Goldberg, and I. V. Mitchell, "Polarization insensitive InGaAS/InGaAsP/InP amplifiers using quantum well intermixing," *Appl. Phys. Lett.*, vol. 69, pp. 562–564, 1996.
[14] C. Francis, M. A. Bradley, P. Boucaud, F. H. Julien, and M. Razeghi, "Intermixing of GaInP/GaAs multiple quantum wells," *Appl. Phys. Lett.*, vol. 62, pp. 178–180, 1993.
[15] W. X. Zou, J. L. Merz, R. J. Fu, and C. S. Hong, "Very-low-threshold, strained $In_yGa_{1-y}As$-GaAs quantum-well lasers defined by impurity-induced disordering," *IEEE Photon. Technol. Lett.*, vol. 3, pp. 400–402, 1991.
[16] P. J. A. Thijs, L. F. Tiemeijer, J. J. M. Binsma, and T. van Dongen, "Progress in long-wavelength strained-layer InGaAs(P) quantum-well semiconductor lasers and amplifiers," *IEEE J. Quantum Electron.*, vol. 30, pp. 477–499, 1994.
[17] H. Ribot, K. W. Lee, R. J. Simes, R. H. Yan, and L. A. Coldren, "Disordering of GaAs/AlGaAs multiple quantum well structures by thermal annealing for monolithic integration of laser and phase modulator," *Appl. Phys. Lett.*, vol. 55, pp. 672–674, 1989.
[18] A. G. Steele, M. Buchanan, H. C. Liu, and Z. R. Wasilewski, "Post-growth tuning of quantum-well infrared detectors by rapid thermal annealing," *J. Appl. Phys.*, vol. 75, pp. 8234–8236, 1994.
[19] A. Ramdane, P. Krauz, E. V. K. Rao, A. Kamoudi, A. Ougazzaden, D. Robein, A. Gloukhian, and M. Carré, "Monolithic integration of InGaAsP-InP strained-layer distributed feedback laser and external modulator by selective quantum-well interdiffusion," *IEEE Photon. Technol. Lett.*, vol. 7, pp. 1016–1018, 1995.
[20] H. Asai and K. Oe, "Energy band-gap shift with elastic strain in $Ga_xIn_{1-x}P$ epitaxial layers grown on (001) GaAs substrates," *J. Appl. Phys.*, vol. 54, pp. 2052–2056, 1983.
[21] G. Ji, D. Huang, U. K. Reddy, T. S. Henderson, R. Houdré, and H. Morkoç, "Optical investiagtion of highly strained InGaAs-GaAs multiple quantum wells," *J. Appl. Phys.*, vol. 62, pp. 3366–3373, 1987.
[22] T. E. Schlesinger and T. Kuech, "Determination of the interdiffusion of Al and Ga in undoped (Al,Ga)As/GaAs quantum well," *Appl. Phys. Lett.*, vol. 49, pp. 519–521, 1986.
[23] D. J. BenDaniel and C. B. Duke, "Space-charge effects on electron tunneling," *Phys. Rev.*, vol. 152, pp. 683–692, 1966.
[24] G. Bastard, J. B. Brum, and R. Ferreira, *Solid State Physics—Advances in Research and Applications*, H. Ehrenreich and D. Turnbull, Eds. New York: Academic, 1991, vol. 44, p. 232.
[25] J. Micallef, E. H. Li, and B. L. Weiss, "Effect of interdiffusion on the sub-band edge structure of $In_{0.53}Ga_{0.47}As$/InP single quantum wells," *J. Appl. Phys.*, vol. 73, pp. 7524–7532, 1993.
[26] M. S. Faleh, J. Tasselli, J. P. Bailbe, and A. Marty, "Transistor-based evaluation of conduction-band offset in GaInP/GaAs heterojunction," *Appl. Phys. Lett.*, vol. 69, pp. 1288–1290, 1996.
[27] T. J. Lee, P. A. Houston, R. Kumar, X. F. Yang, G. Hill, M. Hopkinson, and P. A. Claxton, "Conduction-band discontinuity in InGaP/GaAs measured using both current-voltage and photoemission," *Appl. Phys. Lett.*, vol. 60, pp. 474–476, 1992, and references therein.
[28] S. D. Gunapala, B. F. Levine, R. A. Logan, T. Tanbun-Ek, and D. A. Humphrey, "GaAs/GaInP multiquantum well long-wavelength infrared detector using bound-to-continuum state absorption," *Appl. Phys. Lett.*, vol. 57, pp. 1802–1804, 1990.
[29] J. R. Hoff, M. Razeghi, and G. J. Brown, "Effect of spin spilt-off band on optical absorption in p-type $Ga_{1-x}In_xAs_yP_{1-y}$ quantum-well infrared detectors," *Phys. Rev. B*, vol. 54, pp. 10773–10783, 1996.
[30] G. P. Kothiyal and P. Bhattacharya, "Optical properties and Stokes shifts in lamp-annealed InGaAs/GaAs strained layer superlattices," *J. Appl. Phys.*, vol. 63, pp. 2760–2764, 1988.
[31] H. Temkin, S. N. G. Chu, M. B. Panish, and R. A. Logan, "Thermal stability of InGaAs/InP quantum well structures grown by gas source molecular beam epitaxy," *Appl. Phys. Lett.*, vol. 50, pp. 956–958, 1987.
[32] L. F. Tiemeijer, P. J. A. Thijs, A. J. de Waard, J. J. M. Binsma, and T. v. Dongen, "Dependence of polarization, gain, linewidth enhancement factor, and K factor on the sign of strain of InGaAs/InP strained-layer multiquantum well lasers," *Appl. Phys. Lett.*, vol. 58, pp. 2738–2740, 1991.

Joseph Micallef (M'92), photograph and biography not available at the time of publication.

Andrea Brincat, photograph and biography not available at the time of publication.

Wai-Chee Shiu, photograph and biography not available at the time of publication.